SZABO SCANDIC

Part of Europa Biosite

Produktinformation

- Forschungsprodukte & Biochemikalien
- Zellkultur & Verbrauchsmaterial
- Diagnostik & molekulare Diagnostik
- Laborgeräte & Service

Weitere Information auf den folgenden Seiten!
See the following pages for more information!

Lieferung & Zahlungsart

siehe unsere Liefer- und Versandbedingungen

Zuschläge

- Mindermengenzuschlag
- Trockeneiszuschlag
- Gefahrgutzuschlag
- Expressversand

SZABO-SCANDIC HandelsgmbH

Quellenstraße 110, A-1100 Wien

T. +43(0)1 489 3961-0

F. +43(0)1 489 3961-7

mail@szabo-scandic.com

www.szabo-scandic.com

linkedin.com/company/szaboscandic

Datasheet for 600-101-215M

GFP Antibody

Overview

Description:	Anti-GFP (GOAT) Antibody - 600-101-215M
Item No.:	600-101-215M
Size:	100 µg
Applications:	ELISA, IF, WB, EM, FC, FISH, IHC, IP, Multiplex, Other, Purification
Reactivity:	GFP, eGFP, rGFP
Host Species:	Goat

Product Details

Background:	Green fluorescent protein is a 27 kDa protein produced from the jellyfish Aequorea victoria, which emits green light (emission peak at a wavelength of 509nm) when excited by blue light. GFP is an important tool in cell biology research. GFP is widely used enabling researchers to visualize and localize GFP-tagged proteins within living cells without the need for chemical staining.
Synonyms:	goat anti-GFP antibody, GFP, Green Fluorescent Protein, GFP antibody, Green Fluorescent Protein antibody, EGFP, enhanced Green Fluorescent Protein, Aequorea victoria, Jellyfish
Host Species:	Goat
Clonality:	Polyclonal
Format:	IgG

Target Details

Reactivity:	GFP, eGFP, rGFP
Immunogen Type:	Recombinant Protein
Immunogen:	The immunogen is a Green Fluorescent Protein (GFP) fusion protein corresponding to the full length amino acid sequence (246aa) derived from the jellyfish Aequorea victoria.

Purity/Specificity:	GFP antibody was prepared from monospecific antiserum by immunoaffinity chromatography using Green Fluorescent Protein (Aequorea victoria) coupled to agarose beads followed by solid phase adsorption(s) to remove any unwanted reactivities. Assay by immunoelectrophoresis resulted in a single precipitin arc against anti-Goat Serum and purified and partially purified Green Fluorescent Protein (Aequorea victoria). No reaction was observed against Human, Mouse or Rat serum proteins.
Relevant Links:	• 600-101-215 SDS • UniProtKB - P42212

Application Details

Tested Applications:	ELISA, IF, WB
Suggested Applications:	EM, FC, FISH, IHC, IP, Multiplex, Other, Purification (Based on references)
Application Note:	Anti-GFP is designed to detect GFP and its variants. Goat Anti-GFP has been tested by ELISA, Western blot, and immunofluorescence. This product is also suitable for EM, FC, FISH, IHC, IP, purification, and multiplex assays based on published references. This antibody can be used to detect GFP by ELISA (sandwich or capture) for the direct binding of antigen and recognizes wild-type, recombinant, and enhanced forms of GFP. Researchers should determine optimal titers for applications.
Assay Dilutions:	All assays should be optimized by the user. Recommended dilutions (if any) may be listed below.
ELISA:	1:20,000
IF:	1:500
IHC:	1:200 - 1:1,000
IP:	yes
WB:	1:400-1:2,000
Other:	FISH, Immuno-EM, TEM

Formulation

Physical State:	Liquid (sterile filtered)
Concentration:	1.18 mg/mL by UV absorbance at 280 nm
Buffer:	0.02 M Potassium Phosphate, 0.15 M Sodium Chloride, pH 7.2
Preservative:	0.01% (w/v) Sodium Azide
Stabilizer:	None

Shipping & Handling

Shipping Condition:	Dry Ice
Storage Condition:	Store GFP antibody at -20° C prior to opening. Aliquot contents and freeze at -20° C or below for extended storage. Avoid cycles of freezing and thawing. Centrifuge product if not completely clear after standing at room temperature. This product is stable for several weeks at 4° C as an undiluted liquid. Dilute only prior to immediate use.
Expiration:	Expiration date is one (1) year from date of receipt.

Images

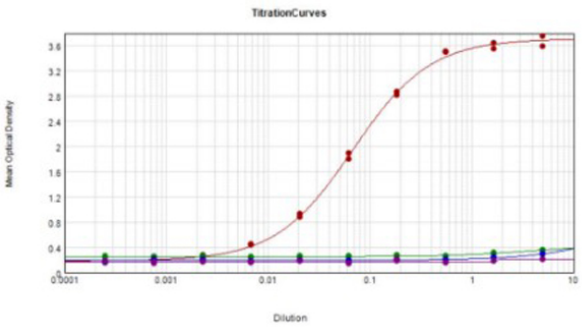

ELISA
ELISA results of purified Goat Anti-GFP Antibody mx3. Each well was coated in 1.0 µg of antigen GFP [Red Line], human IgG [Green Line], Mouse IgG [Blue Line], and Rat IgG [Purple Line]. The starting dilution of antibody was 5 µg/mL and the X-axis represents the Log10 of a 3-fold dilution. The titer is 1:14,800. This titration is a 4-parameter curve fit where the IC50 is defined as the titer of the antibody. Assay performed using Buffer (p/n MB-060-1000), Substrate (p/n TMB-8000), and Donkey Anti-Goat IgG Antibody HRP (p/n 605-703-125).

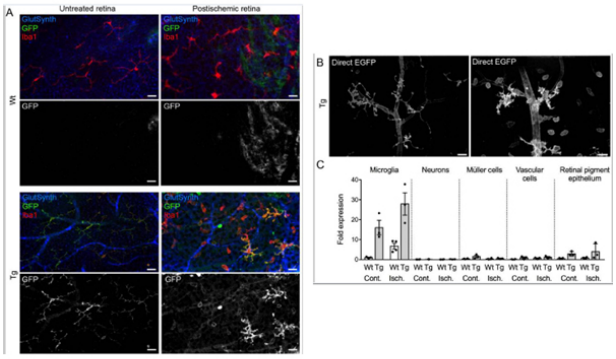

Immunofluorescence Microscopy

Upregulation of P2X7 expression in postischemic retinae 3 days post injury (dpi) of wt and P2X7-EGFP transgenic animals. (A) Retinal flat mount scanned at the plane of the ganglion cell layer (GCL) to delineate microglia residing in this retinal layer. Co-labeling for GFP (600-101-215, Rockland), Iba1 (marker for microglia/macrophages) and glutamine synthetase (marker for Müller glia) shows that EGFP exclusively co-localizes with microglia and in the postischemic retina also with morphologically distinct Iba1-positive cells that likely correspond to infiltrated macrophages. Note unspecific vessel staining caused by the secondary antibody against glutamine synthetase. Scale bars: 20 µm. n = 2 individual line 61 in FVB/C57b/6 hybrid mice. (B) Direct EGFP-fluorescence captured at identical microscope settings in non-fixed retinal flatmounts focused on the GCL shows increased EGFP signal in vessels and microglia and an increase in the number of microglia and/or macrophages. Scale bar: 20 µm. (C) P2X7 expression determined by quantitative real-time PCR on the indicated cell types isolated by immunomagnetic separation from control and postischemic (3 dpi) retinae of line 17 P2X7-EGFP transgenic mice in (C57b/6 background). Bars represent mean ±SEM and include data from 3 to 4 animals/each genotype/condition. Significance between expression level in the untreated control eye of the respective genotype was analyzed using unpaired two-tailed Mann-Whitney-U-test and indicated as: *p<0.05. Data were normalized to the housekeeper pyruvate dehydrogenase beta (PDHB) and results are presented as relative expression levels compared to that in microglia of healthy wild-type retinae. Increase in P2X7 signal in RPE is most likely due to contamination by infiltrating immune cells. Figure provided by CiteAb. Source: Elife, PMID: 30074479.

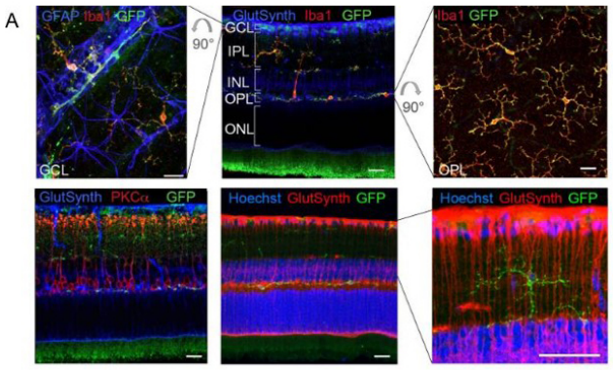

Immunofluorescence Microscopy

P2X7-EGFP expression in retina, sciatic nerves, spinal cord, and at the neuromuscular synapse. (A) EGFP exclusively co-localizes with microglia and endothelial cells in the adult mouse retina. Upper panel: Middle, retinal slice labeled for GFP (600-101-215, Rockland), Iba1 (marker for microglia/macrophages) and glutamine synthetase (marker for Müller glia). Left and right, retinal flat mounts scanned at the plane of the ganlion cell layer (GCL) and outer plexiform layer (OPL), respectively, to delineate microglia residing in these retinal layers. Astrocytes in the GCL were labeled with GFAP. IPL, inner plexiform layer; INL, inner nuclear layer; ONL, outer nuclear layer. Lower panel: Co-staining of EGFP with neuronal marker PKCα (left) and glutamine synthetase (two right panels) at higher contrast and resolution to show absence of neuronal P2X7-EGFP. Cell nuclei were counterstained with Hoechst 33342 (blue) Scale bars: 20 µm. n = 2 individual line 61 in FVB/C57b/6 hybrid mice. Figure provided by CiteAb. Source: Elife, PMID: 30074479.

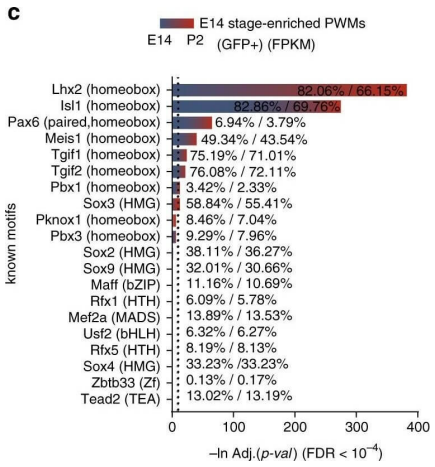

Flow Cytometry

Binding sites for transcription factors with predicted pioneer function co-occur with LHX2 peaks. (a, b) Hierarchical clustering of LHX2 ChIP-Seq regulatory motifs and assigned representative logos are represented at E14 (a) and P2 (b) (linkage = average; similarity threshold cor = 0.6, ncor = 0.4, w = 5). The most enriched cluster comprises LHX2 and multiple variations of the same motif. (c, d) Known transcription factor motifs preferentially enriched in either E14 or P2 LHX2 ChIP-Seq peaks and identified by pairwise comparison are shown. Percentage of motif occurrences are reported for input and background datasets. The relative expression level of the corresponding transcription factor mRNA at E14/P2 is indicated by the blue/red color gradient, respectively Figure provided by CiteAb. Source: Commun Biol, PMID: 31044167.

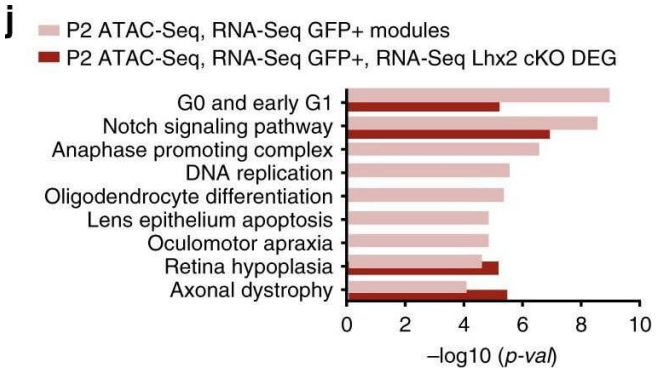

Flow Cytometry

LHX2 regulates cell cycle genes and the Notch signaling pathway by targeting promoters and non-coding elements in nucleosome free regions associated with active enhancers. A) LHX2 motif density around the centers of ChIP-Seq peaks at E14 and P2. B) Enrichment of LHX2 ChIP-Seq peaks distributed across different genomic regions (log2 fold enrichment). (C-F) Percentage of LHX2 target genes in retinal term assigned to at least one age-matched LHX2 ChIP-Seq peak. Enrichment was computed between target genes in term and total number of known genes in term (Supplementary Table 4 and Supplementary Data 1) for peaks shared at E14 and P2 (C), stage-specific peaks (D), and all peaks detected at E14 (E) and P2 (F). RNA-Seq from age-matched Lhx2 cKO retinas identifies Lhx2-dependent genes sets. (*p-value < 0.05, ***p-value < 0.001). Asterisks in parenthesis refer to p-values before Bonferroni–Hochberg correction (target genes populating the enriched ontologies are in Supplementary Data 2). (G, H) Heatmaps of raw reads from LHX2 ChIP-Seq peaks are plotted across nucleosome centered regions from age-matched ATAC-Seq samples. Each row represents a 3 kb window centered at maximum read pile-up. LHX2 motif occurrence in open chromatin regions is displayed and reported in Supplementary Tables 6. LHX2 motifs co-localize with RNA-Seq raw reads. Meta-profiles of the class II enhancer-associated H3K27ac marks were compiled at bidirectionally transcribed regions from the E14 (G) and P2 RPCs fractions (H) (background in gray, opposite strands replicates in hue). (I, J) Functional enrichment of Lhx2-dependent genes sets encoded within open chromatin regions (Supplementary Tables 6) by binomial distribution Figure provided by CiteAb. Source: Commun Biol, PMID: 31044167.

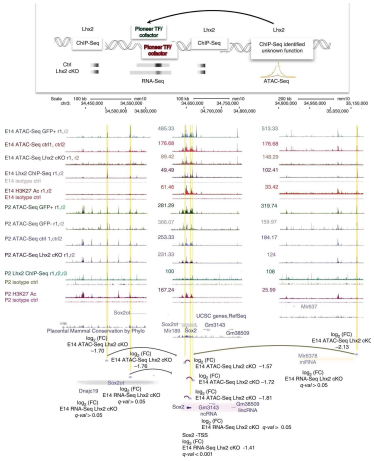

Flow Cytometry

LHX2 coordinates variations in chromatin accessibility at the Sox2 locus. Custom tracks of E14 and P2 LHX2 ChIP-Seq reads and age-matched ATAC-Seq from purified RPCs and post mitotic precursors were configured on the mm10 UCSC murine genome assembly. Regions of interest targeted by LHX2, where variations by RNA-Seq and/or ATAC-Seq coverage are observed in Lhx2 cKO retinas are highlighted. Association with H3K27ac-labeled enhancer elements is also indicated. The LHX2-coordinated regulatory module is defined as follows: regulatory regions that display variations in ATAC-Seq coverage without a corresponding variation in the nearest transcript by E14 Lhx2 cKO RNA-Seq are putatively assigned (arrows) to the nearest gene exhibiting variation in transcript levels Figure provided by CiteAb. Source: Commun Biol, PMID: 31044167.

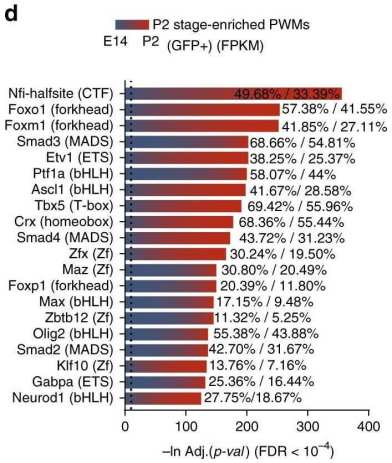

Flow Cytometry

Binding sites for transcription factors with predicted pioneer function co-occur with LHX2 peaks. a, b Hierarchical clustering of LHX2 ChIP-Seq regulatory motifs and assigned representative logos are represented at E14 (a) and P2 (b) (linkage = average; similarity threshold cor = 0.6, ncor = 0.4, w = 5). The most enriched cluster comprises LHX2 and multiple variations of the same motif. (c, d) Known transcription factor motifs preferentially enriched in either E14 or P2 LHX2 ChIP-Seq peaks and identified by pairwise comparison are shown. Percentage of motif occurrences are reported for input and background datasets. The relative expression level of the corresponding transcription factor mRNA at E14/P2 is indicated by the blue/red color gradient, respectively Figure provided by CiteAb. Source: Commun Biol, PMID: 31044167.

i

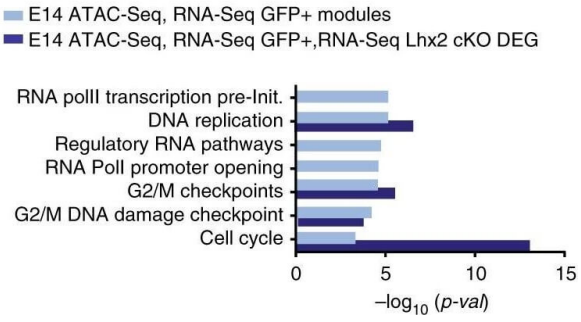

Flow Cytometry

LHX2 regulates cell cycle genes and the Notch signaling pathway by targeting promoters and non-coding elements in nucleosome free regions associated with active enhancers. a LHX2 motif density around the centers of ChIP-Seq peaks at E14 and P2. b Enrichment of LHX2 ChIP-Seq peaks distributed across different genomic regions (log2 fold enrichment). c–f Percentage of LHX2 target genes in retinal term assigned to at least one age-matched LHX2 ChIP-Seq peak. Enrichment was computed between target genes in term and total number of known genes in term (Supplementary Table 4 and Supplementary Data 1) for peaks shared at E14 and P2 (c), stage-specific peaks (d), and all peaks detected at E14 (e) and P2 (f). RNA-Seq from age-matched Lhx2 cKO retinas identifies Lhx2-dependent genes sets. (*p-value < 0.05, ***p-value < 0.001). Asterisks in parenthesis refer to p-values before Bonferroni–Hochberg correction (target genes populating the enriched ontologies are in Supplementary Data 2). g, h Heatmaps of raw reads from LHX2 ChIP-Seq peaks are plotted across nucleosome centered regions from age-matched ATAC-Seq samples. Each row represents a 3 kb window centered at maximum read pile-up. LHX2 motif occurrence in open chromatin regions is displayed and reported in Supplementary Tables 6. LHX2 motifs co-localize with RNA-Seq raw reads. Meta-profiles of the class II enhancer-associated H3K27ac marks were compiled at bidirectionally transcribed regions from the E14 (g) and P2 RPCs fractions (h) (background in gray, opposite strands replicates in hue). i, j Functional enrichment of Lhx2-dependent genes sets encoded within open chromatin regions (Supplementary Tables 6) by binomial distribution Figure provided by CiteAb. Source: Commun Biol, PMID: 31044167.

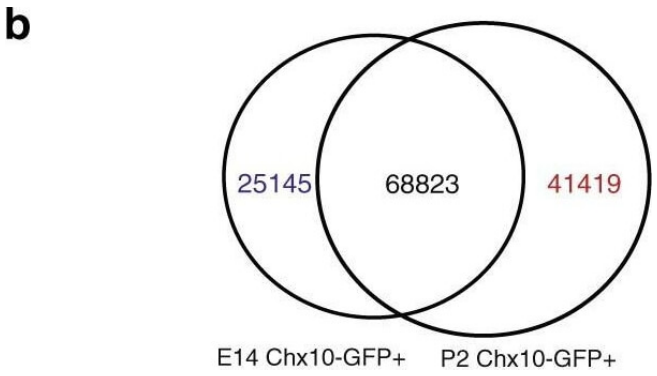

Flow Cytometry

Pairwise comparison of ATAC-Seq data identifies open chromatin regions from early and late RPCs, with a broad overrepresentation of LHX2 related motifs. A) Workflow for epigenomic profiling of RPC. B) Venn-diagram represents open chromatin regions identified in early- and late-stage VSX2 (CHX10)—GFP-positive RPCs. C) Hierarchical clustering of known motifs in the vertebrate genome (left, Jaspar 2016 non-redundant vertebrates core). Inset represents the major cluster of probabilistically assigned position weight matrices (PWMs) identified in open chromatin regions from early- and late-stage RPCs (scale = 1 node/pixel) (linkage = average; similarity threshold cor = 0.6, ncor = 0.4, w = 5) (Lhx2 instances as blue pixel strokes). D) Relative RNA-Seq expression for homeobox transcription factors. E) Representative LHX2 logos (MA0700.1, k-mer sig = 300, e-value = 1e-300), with positional variations of the same motif instance. F) Known motifs enrichment in open chromatin regions from early and late RPCs by binomial scoring of PWMs. G) LHX2 footprints from open chromatin regions identified in early- and late-stage RPCs. H) Custom tracks of RPC-derived ATAC-Seq profiles and aged-matched LHX2 ChIP-Seq feature the Vsx2 locus (mm9). Figure provided by CiteAb. Source: Commun Biol, PMID: 31044167.

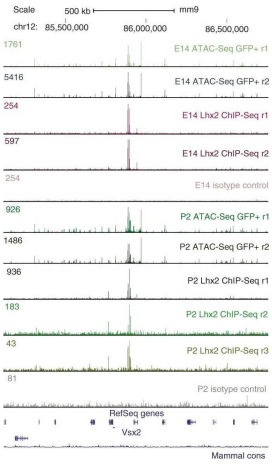

Flow Cytometry

Pairwise comparison of ATAC-Seq data identifies open chromatin regions from early and late RPCs, with a broad overrepresentation of LHX2 related motifs. A) Workflow for epigenomic profiling of RPC. B) Venn-diagram represents open chromatin regions identified in early- and late-stage VSX2 (CHX10)—GFP-positive RPCs. C) Hierarchical clustering of known motifs in the vertebrate genome (left, Jaspar 2016 non-redundant vertebrates core). Inset represents the major cluster of probabilistically assigned position weight matrices (PWMs) identified in open chromatin regions from early- and late-stage RPCs (scale = 1 node/pixel) (linkage = average; similarity threshold cor = 0.6, ncor = 0.4, w = 5) (Lhx2 instances as blue pixel strokes). D) Relative RNA-Seq expression for homeobox transcription factors. E) Representative LHX2 logos (MA0700.1, k-mer sig = 300, e-value = 1e-300), with positional variations of the same motif instance. F) Known motifs enrichment in open chromatin regions from early and late RPCs by binomial scoring of PWMs. G) LHX2 footprints from open chromatin regions identified in early- and late-stage RPCs. H) Custom tracks of RPC-derived ATAC-Seq profiles and aged-matched LHX2 ChIP-Seq feature the Vsx2 locus (mm9). Figure provided by CiteAb. Source: Commun Biol, PMID: 31044167.

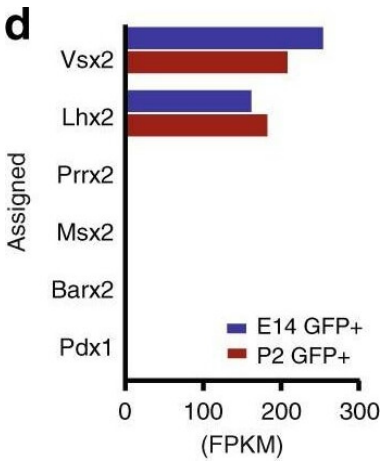

Flow Cytometry

Pairwise comparison of ATAC-Seq data identifies open chromatin regions from early and late RPCs, with a broad overrepresentation of LHX2 related motifs. A) Workflow for epigenomic profiling of RPC. B) Venn-diagram represents open chromatin regions identified in early- and late-stage VSX2 (CHX10)—GFP-positive RPCs. C) Hierarchical clustering of known motifs in the vertebrate genome (left, Jaspar 2016 non-redundant vertebrates core). Inset represents the major cluster of probabilistically assigned position weight matrices (PWMs) identified in open chromatin regions from early- and late-stage RPCs (scale = 1 node/pixel) (linkage = average; similarity threshold cor = 0.6, ncor = 0.4, w = 5) (Lhx2 instances as blue pixel strokes). D) Relative RNA-Seq expression for homeobox transcription factors. E) Representative LHX2 logos (MA0700.1, k-mer sig = 300, e-value = 1e-300), with positional variations of the same motif instance. F) Known motifs enrichment in open chromatin regions from early and late RPCs by binomial scoring of PWMs. G) LHX2 footprints from open chromatin regions identified in early- and late-stage RPCs. H) Custom tracks of RPC-derived ATAC-Seq profiles and aged-matched LHX2 ChIP-Seq feature the Vsx2 locus (mm9). Figure provided by CiteAb. Source: Commun Biol, PMID: 31044167.

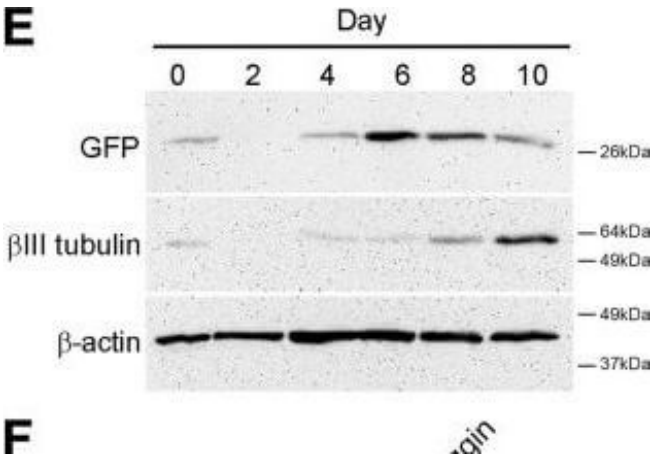

Western Blot

Npas4 expression during neural differentiation of ESCs. (A) RT-PCR analysis was used to determine the temporal expression profile of Npas4 mRNA in relation to various marker genes during N2B27 differentiation of mESCs (n = 3). Primers to the reference gene β-actin were used as a loading control. The negative control reaction (−) contained water in place of template cDNA. (B) The changes in Npas4 expression during N2B27 differentiation were quantified using qRT-PCR. At each time point Npas4 expression was normalized to β-actin expression and fold changes are relative to Day 0 (undifferentiated mESCs). Mean values and standard deviations of three independent experiments (n = 3) are displayed. (C)In situ hybridization analysis of Npas4 mRNA expression at Day 4 of N2B27 differentiation of mESCs. Representative images of differentiating colonies from two independent experiments (n = 2) are shown. Top panel - Npas4 antisense probe; Bottom panel - Npas4 sense probe. Scale bar = 100 µm. (D) Immunoblotting was used to determine the temporal expression profile of the Npas4 protein during N2B27 differentiation of mESCs. An antibody to the reference protein β-actin was used as a loading control (n = 3). (E) Immunoblotting was used to determine the temporal expression profile of Sox1 in the 46C cell line (using an antibody to GFP) and βIII tubulin during N2B27 differentiation of mESCs. An antibody to the reference protein β-actin was used as a loading control (n = 3). (F) RT-PCR analysis of NPAS4 mRNA in relation to various marker genes during Noggin-induced neural differentiation of hESCs (n = 3). Primers to the reference gene β-ACTIN were used as a loading control. The negative control reaction (−) contained water in place of template cDNA. hESCs, human embryonic stem cells; mESCs, mouse embryonic stem cells; NS, neurospheres. Figure provided by CiteAb. Source: Stem Cell Res Ther, PMID: 24887558.

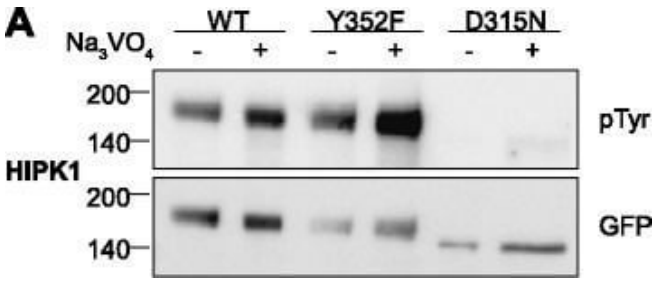

Western Blot
Tyrosine phosphorylation of HIPK mutants. HeLa cells were transiently transfected with the indicated expression constructs for HIPK1 (A), HIPK2 (B), HIPK3 (C) or HIPK4 (D). Sodium orthovanadate (Na3VO4) was added to every second sample for 1 h before lysis. GFP fusion proteins were immunoprecipitated and analysed by immunodetection with antibodies for pTyr and GFP. The panels are representative of 2–3 independent experiments. Figure provided by CiteAb. Source: Cell Commun Signal, PMID: 25630557.

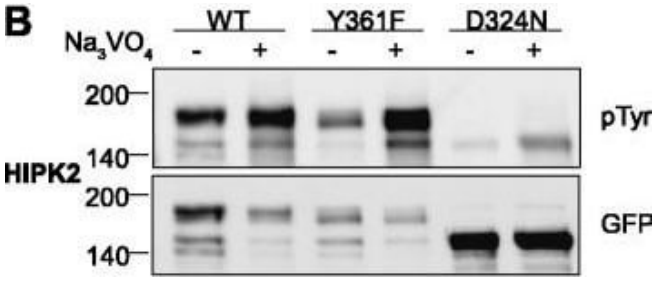

Western Blot
Tyrosine phosphorylation of HIPK mutants. HeLa cells were transiently transfected with the indicated expression constructs for HIPK1 (A), HIPK2 (B), HIPK3 (C) or HIPK4 (D). Sodium orthovanadate (Na3VO4) was added to every second sample for 1 h before lysis. GFP fusion proteins were immunoprecipitated and analysed by immunodetection with antibodies for pTyr and GFP. The panels are representative of 2–3 independent experiments. Figure provided by CiteAb. Source: Cell Commun Signal, PMID: 25630557.

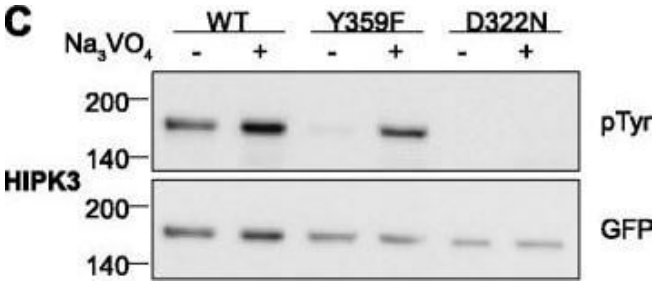

Western Blot
Tyrosine phosphorylation of HIPK mutants. HeLa cells were transiently transfected with the indicated expression constructs for HIPK1 (A), HIPK2 (B), HIPK3 (C) or HIPK4 (D). Sodium orthovanadate (Na3VO4) was added to every second sample for 1 h before lysis. GFP fusion proteins were immunoprecipitated and analysed by immunodetection with antibodies for pTyr and GFP. The panels are representative of 2–3 independent experiments. Figure provided by CiteAb. Source: Cell Commun Signal, PMID: 25630557.

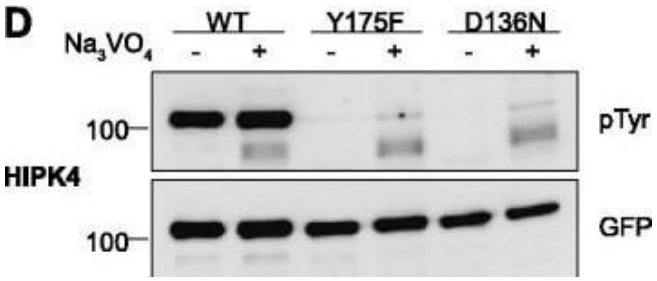

Western Blot
Tyrosine phosphorylation of HIPK mutants. HeLa cells were transiently transfected with the indicated expression constructs for HIPK1 (A), HIPK2 (B), HIPK3 (C) or HIPK4 (D). Sodium orthovanadate (Na3VO4) was added to every second sample for 1 h before lysis. GFP fusion proteins were immunoprecipitated and analysed by immunodetection with antibodies for pTyr and GFP. The panels are representative of 2–3 independent experiments. Figure provided by CiteAb. Source: Cell Commun Signal, PMID: 25630557.

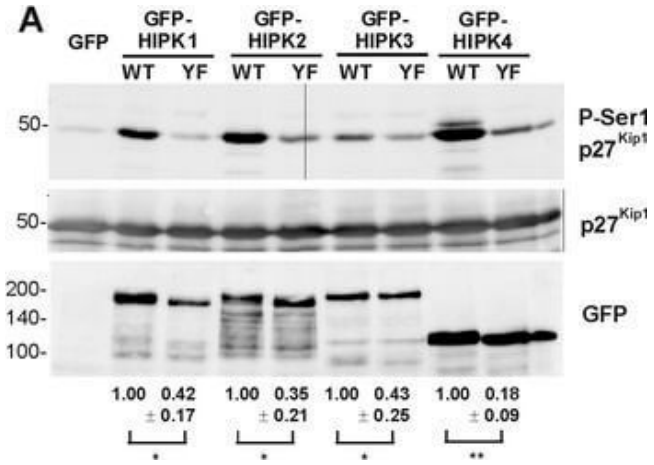

Western Blot
Maximal activity of HIPKs depends on the activation loop tyrosine. Wild type GFP-HIPK fusion proteins and the respective Tyr→Phe mutants were immunoprecipitated from HeLa cells and subjected to kinase assays with recombinant GST-p27Kip1(A), myelin basic protein (B) or DYRKtide (C). GFP served as background control. A, Phosphorylation of p27Kip1 at Ser10 was detected by immunoblotting with a phosphorylation-specific antibody. For quantitative evaluation, pSer10 immunoreactivity was normalised to GFP immunoreactivity, which reflects the amount of kinase in the reaction. The blots illustrate a representative experiment, and the relative catalytic activities as determined from 3–4 assays are shown below the panels (means ± SD). One-sample t test: *, $p < 0.05$; **, $p < 0.01$. B and C, Phosphorylation of MBP and DYRKtide was measured in triplicate as incorporation of 32P. Background values from the GFP control samples were subtracted and activities were normalised to the amount of kinase in the reaction as determined by GFP immunoreactivity. Column diagrams illustrate catalytic activities relative to HIPK2 (WT). The results were replicated in independent experiments, except for a missing value of HIPK1. Figure provided by CiteAb. Source: Cell Commun Signal, PMID: 25630557.

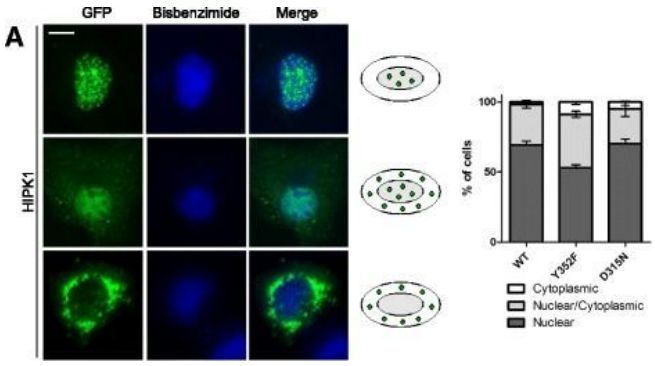

Immunocytochemistry
Subcellular distribution of HIPK mutants. COS-7 cells were transfected with expression vectors for GFP-HIPK1 (A), GFP-HIPK2 (B), GFP-HIPK3 (C) or GFP-HIPK4 (D). The cellular localisation of the HIPK constructs was evaluated by imaging GFP autofluorescence in relation to bisbenzimide-stained nuclei. For each kinase, cells were classified into 3 major patterns that are illustrated by representative images and icons. The cells shown were transfected with (top to bottom) HIPK1 WT, DN, YF; HIPK2 WT, WT, YF; HIPK3 WT, WT, DN and HIPK4 DN, DN. A series of images of the different patterns for each kinase and its mutants is provided in the additional material (Additional file 1: Figure S3). Here the graphs show the percentages of cells classified into the indicated patterns (means ± SD, n = 3). In each of 3 experiments, at least 90 cells were evaluated for all HIPK constructs. Scale bars, 10 µm. Figure provided by CiteAb.
Source: Cell Commun Signal, PMID: 25630557.

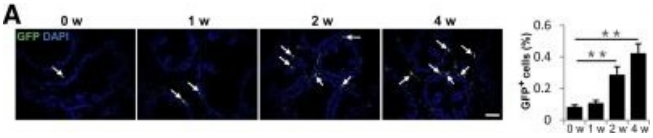

Immunohistochemistry

Increased nestin+ cells in prostate stroma are a subset of mesenchymal/stromal stem cells. (A): Immunofluorescence analysis of prostate tissue sections from Nestin-GFP transgenic mice at 0, 1, 2, and 4 weeks after initial PE injection using antibody against GFP. Arrows indicate GFP+ cells. Bar graph on the right shows the quantitative analyses of the ratio of GFP+ cells to total cells. Scale bar = 50μm. (B): Double-immunohistofluorescence analysis of prostate tissue sections from Nestin-GFP mice using antibodies against GFP and CD90 or Sca1. Scale bar = 20 μm. (C): Flow cytometry analysis of GFP+CD45–cells (percentage of total cells counted) in blood of Nestin-GFP mice at indicated time points after PE injection. (D): Flow cytometry analysis of CD90+Sca1+CD11b–CD45– cells (percentage of total cells counted) in blood of wild-type mice at indicated time points after PE injection. (E): Fluorescence-activated cell sorting of GFP+CD45−cells from ventral prostate tissue of 6-week-old Nestin-GFP mice. (F): Single CFU-F-derived GFP+CD45− cell strains were isolated and individually expanded for characterization assays. (G): Single GFP+CD45− clones were isolated, expanded, and cultured. Cells were separately incubated with fibrogenic media, osteogenic media, adipogenic media, and chondrogenic media, and they were stained for vimentin (upper left panel), Alizarin Red S (upper right panel), Oil Red O (lower left panel), and Toluidine Blue (lower right panel), respectively. (H): Double-immunohistofluorescence analysis of prostate tissue sections from 6-week-old Nestin-Cre, Rosa26-YFPflox/+ mice using antibodies against YFP (green) and vimentin (red, top panels) or α-SMA (red, bottom panels). Scale bar = 50μm. n = 4–5 per group. Data are shown as the mean ± SD. ⍰, $p < .05$, ⍰⍰, $p < .01$ determined by multifactorial analysis of variance. Abbreviations: CFU-F, colony-forming unit fibroblast; DAPI, 4’,6-diamidino-2-phenylindole; GFP, green fluorescent protein; PE, phenylephrine; α-SMA, α-smooth muscle actin; w, weeks. Figure provided by CiteAb. Source: Stem Cells Transl Med, PMID: 28191756.

Immunohistochemistry

Increased nestin+ cells in prostate stroma are a subset of mesenchymal/stromal stem cells. (A): Immunofluorescence analysis of prostate tissue sections from Nestin-GFP transgenic mice at 0, 1, 2, and 4 weeks after initial PE injection using antibody against GFP. Arrows indicate GFP+ cells. Bar graph on the right shows the quantitative analyses of the ratio of GFP+ cells to total cells. Scale bar = 50µm. (B): Double-immunohistofluorescence analysis of prostate tissue sections from Nestin-GFP mice using antibodies against GFP and CD90 or Sca1. Scale bar = 20 µm. (C): Flow cytometry analysis of GFP+CD45–cells (percentage of total cells counted) in blood of Nestin-GFP mice at indicated time points after PE injection. (D): Flow cytometry analysis of CD90+Sca1+CD11b–CD45– cells (percentage of total cells counted) in blood of wild-type mice at indicated time points after PE injection. (E): Fluorescence-activated cell sorting of GFP+CD45−cells from ventral prostate tissue of 6-week-old Nestin-GFP mice. (F): Single CFU-F-derived GFP+CD45− cell strains were isolated and individually expanded for characterization assays. (G): Single GFP+CD45− clones were isolated, expanded, and cultured. Cells were separately incubated with fibrogenic media, osteogenic media, adipogenic media, and chondrogenic media, and they were stained for vimentin (upper left panel), Alizarin Red S (upper right panel), Oil Red O (lower left panel), and Toluidine Blue (lower right panel), respectively. (H): Double-immunohistofluorescence analysis of prostate tissue sections from 6-week-old Nestin-Cre, Rosa26-YFPflox/+ mice using antibodies against YFP (green) and vimentin (red, top panels) or α-SMA (red, bottom panels). Scale bar = 50µm. n = 4–5 per group. Data are shown as the mean ± SD. □, p < .05, □□, p < .01 determined by multifactorial analysis of variance. Abbreviations: CFU-F, colony-forming unit fibroblast; DAPI, 4’,6-diamidino-2-phenylindole; GFP, green fluorescent protein; PE, phenylephrine; α-SMA, α-smooth muscle actin; w, weeks. Figure provided by CiteAb. Source: Stem Cells Transl Med, PMID: 28191756.

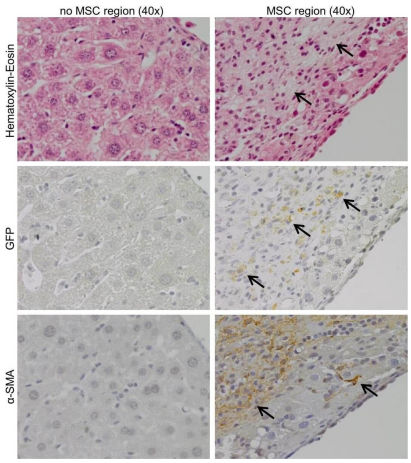

Immunohistochemistry
MSCs are traced in special organized regions. MSC regions and normal regions in regenerated liver tissue of cirrhotic mice treated with pHx + 2 x 106 MSC stained for Haematoxylin-eosin, GFP and α-SMA (40x magnifications, MSCs are indicated by the black arrows). GFP, green fluorescent protein; α-SMA, smooth muscle actin; MSCs, mesenchymal stromal cells; pHx, partial hepatectomy Figure provided by CiteAb. Source: J Cell Mol Med, PMID: 31245923.

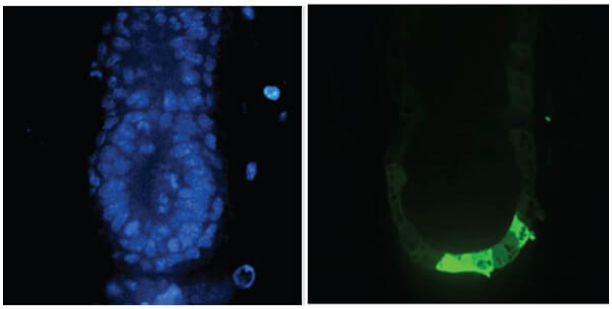

Immunofluorescence Microscopy
Immunofluorescence Microscopy of Anti-GFP (GOAT) Antibody. Tissue: E5.5 Hex-GFP transgenic mouse embryo. Primary antibody: Goat anti-GFP was used at 1:500 dilution. Secondary antibody: Fluorchrome conjugated Anti-goat IgG secondary antibody at 1:10,000 for 45 min at RT. Staining: GFP as green fluorescent signal with DAPI blue counterstain.

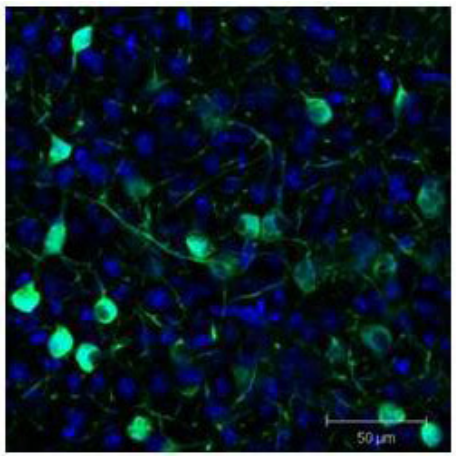

Immunofluorescence Microscopy
Immunofluorescence Microscopy of GFP-GOAT-Antibody. Tissue: Sf-1:Cre mice crossed to the Z/EG reporter line. Mouse brain (coronal view, 20X magnification). Fixation: 4%PFA/PBS with o/n fixation, and subsequently transferred to a 30% sucrose solution. Antigen retrieval: frozen in OCT freezing medium (Sakura) and cryostat sectioned at 40 microns. Primary antibody: Goat anti-GFP was used at 1:500 dilution in free floating imunnohistochemistry to detect GFP. Secondary antibody: Fluorchrome conjugated Anti-goat IgG secondary antibody was used for detection at 1:500 at 1:10,000 for 45 min at RT. Localization: Sf-1+ neurons and their processes of the ventromedial nucleus of the hypothalamus. Staining: eGFP as green fluorescent signal and sections were counterstained with DAPI.

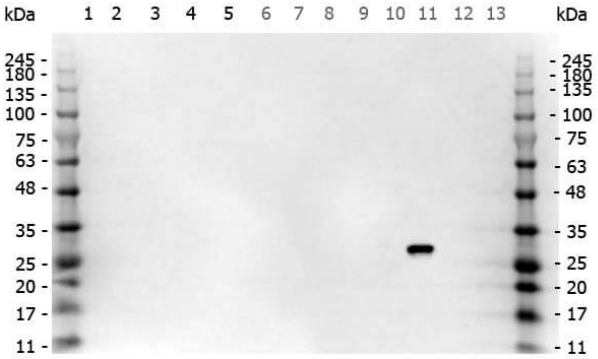

Western Blot

Multi-lysate Western Blot of Goat anti-GFP antibody. Marker: Opal Pre-stained ladder (p/n MB-210-0500). Lane 1: HEK293 lysate (p/n W09-000-365). Lane 2: HeLa Lysate (p/n W09-000-364). Lane 3: CHO/K1 Lysate (p/n W07-000-357). Lane 4: MDA-MB-231 (p/n W09-001-GK6). Lane 5: A431 Lysate (p/n W09-000-361). Lane 6: Jurkat Lysate (p/n W09-001-370). Lane 7: NIH/3T3 Lysate (p/n W10-000-358). Lane 8: E-coli HCP Control (p/n 000-001-J08). Lane 9: FLAG Positive Control Lysate (p/n W00-001-383). Lane 10: Red Fluorescent Protein (p/n 000-001-379). Lane 11: Green Fluorescent Protein (p/n 000-001-215). Lane 12: Glutathione-S-Transferase Protein (p/n 000-001-200). Lane 13: Maltose Binding Protein (p/n 000-001-385). Load: 10 µg of lysate or 50ng of purified protein per lane. Primary antibody: GFP antibody at 1ug/mL overnight at 4C. Secondary antibody: Peroxidase goat secondary antibody at 1:30,000 for 60 min at RT. Blocking Buffer: 1% Casein-TTBS (p/n MB-082) for 30 min at RT. Predicted/Observed size: 30 kDa for GFP.

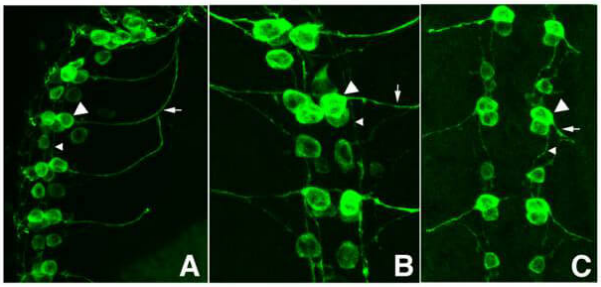

Immunofluorescence Microscopy

Immunofluorescence Microscopy of GFP-GOAT Antibody.
Tissue: Drosophila melanogaster late stage embryonic central nervous system.
Fixation: 0.5% PFA.
Antigen retrieval: not required.
Primary antibody: Anti-GFP antibody at a 1:1,000 for 1 h at RT.
Secondary antibody: AlexaFluor 488™ conjugated Anti-Goat antibody at 1:300 for 45 min at RT.
Panel A: shows a lateral view (ventral left).
Panels B and C: shows ventral views of whole mount embryos at 63x magnification (plus 2x digital zoom).
In all panels, anterior is up.
Staining: tau-GFP cell bodies (large arrowhead) and axons of motorneurons (arrow) and interneurons (small arrowhead) as green fluorescent signal.

Western Blot
Western Blot of Goat anti-GFP antibody. Lane 1: HeLa cells. Lane 2: mock transfected HeLa cell lysate. Load: 35 µg per lane. Primary antibody: GFP antibody at 1 µg/ml for 1 h at room temperature. Secondary antibody: IRDye® 800 conjugated Donkey-a-Goat IgG [H&L] MX7 (605-732-125) secondary antibody at 1:2,500 for 45 min at RT. Block: 5% BLOTTO overnight at 4°C. Predicted/Observed size: 27 kDa, 33 kDa for GFP. Other band(s): none.

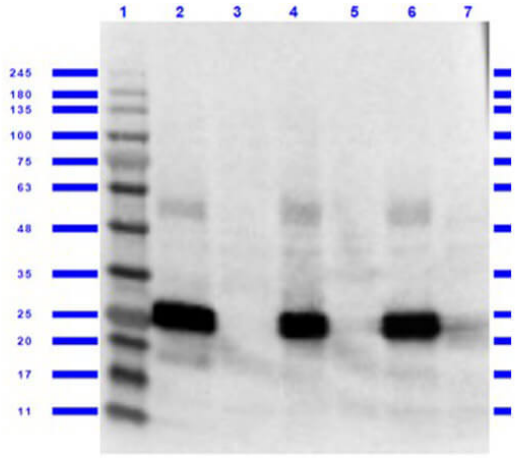

Western Blot
Western Blot of Goat anti-GFP antibody with lysates. Lane 1: Opal Prestained Molecular Weight Marker (p/n MB-210-0500). Lane 2: GFP/HEK293T WCL (p/n 000-001-215/W09-001-GX5) [0.05/10µg]. Lane 3: HEK293T WCL (p/n W09-001-GX5) [10µg]. Lane 4: GFP/NIH-3T3 WCL (p/n 000-001-215/W10-000-358) [0.05/10µg]. Lane 5: NIH-3T3 WCL (p/n W10-000-358) [10µg]. Lane 6: GFP/PC-12 WCL (p/n 000-001 -215/W12-001-GL9) [0.05/10µg]. Lane 7: PC-12 WCL (p/n W12-001-GL9) [10µg]. Primary antibody: Anti-GFP antibody at 1ug/mL overnight at 2-8°C. Secondary antibody: Donkey Anti-Goat IgG HRP secondary antibody (p/n 605-703-002) at 1:40,000 for 30 min at RT. Blocking Buffer: BlockOut Buffer (p/n MB-073) for 1hr at RT. Predicted/Observed size: ~27kDa for GFP.

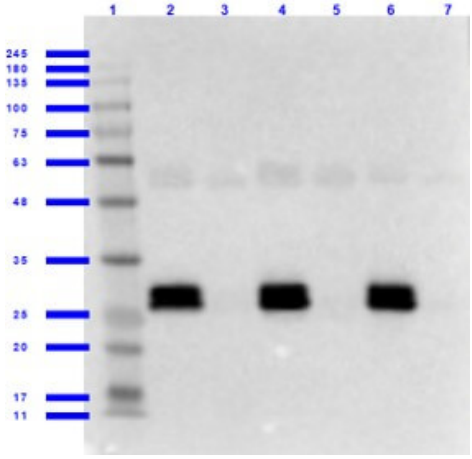

Western Blot
Western Blot of Goat anti-GFP Antibody with Serums. Lane 1: Opal Prestained Molecular Weight Marker (p/n MB-210-0500). Lane 2: GFP/Human Serum (p/n 000-001-215/D314-05) [0.01/0.02µL] [+]. Lane 3: Human Serum (p/n D314-05) [0.02µL] [-]. Lane 4: GFP/Mouse Serum (p/n 000-001-215/D308-05) [0.01/0.02µL] [+]. Lane 5: Mouse Serum (p/n D308-05) [0.02µL] [-]. Lane 6: GFP/Rat Serum (p/n 000-001-215/D310-05) [0.01/0.02µL] [+]. Lane 7: Rat Serum (p/n D310-05) [0.02µL] [-]. Primary antibody: Anti-GFP antibody at 1.0ug/mL overnight at 2-8°C. Secondary antibody: Donkey Anti-Goat IgG HRP secondary antibody (p/n CUSTmx8) at 1:40,000 for 30 min at RT. Blocking Buffer: BlockOut Buffer (p/n MB-073) for 1hr at RT. Predicted/Observed size: ~27kDa for GFP.

References

- El Chehadeh, S et al. SLITRK2 variants associated with neurodevelopmental disorders impair excitatory synaptic function and cognition in mice. *Nature Communications* (2022)
- Zhang, C et al. Autophagic sequestration of SQSTM1 disrupts the aggresome formation of ubiquitinated proteins during proteasome inhibition. *Cell Death & Disease* (2022)
- Omar, MH et al. Mislocalization of protein kinase A drives pathology in Cushing's syndrome. *Cell Reports* (2022)
- Bochyńska, A et al. Induction of senescence upon loss of the Ash2l core subunit of H3K4 methyltransferase complexes. *Nucleic Acids Research* (2022)
- Bin I et al. Human neural progenitors establish a diffusion barrier in the endoplasmic reticulum membrane during cell division. *Development (Cambridge, England)* (2022)
- Choi, YJ et al. The Multivalent Polyampholyte Domain of Nst1, a P-Body-Associated Saccharomyces cerevisiae Protein, Provides a Platform for Interacting with P-Body Components. *International Journal of Molecular Sciences* (2022)
- Chen, PM et al. CD38 reduces mitochondrial fitness and cytotoxic T cell response against viral infection in lupus patients by suppressing mitophagy. *Science Advances* (2022)
- Yshii, L et el. Astrocyte-targeted gene delivery of interleukin 2 specifically increases brain-resident regulatory T cell numbers and protects against pathological neuroinflammation. *Nature Immunology* (2022)
- Guo, L et al. TDP43 promotes stemness of breast cancer stem cells through CD44 variant splicing isoforms. *Cell Death & Disease* (2022)
- DeFlitch, L et al. Age and Alzheimer's Disease-Related Oligodendrocyte Changes in Hippocampal Subregions. *Frontiers in Cellular Neuroscience* (2022)
- Gass, MM et al. PI(4,5)P2 controls slit diaphragm formation and endocytosis in Drosophila nephrocytes. *Cellular and Molecular Life Sciences : Cmls* (2022)
- Hooshdaran, B et al. Stent-based delivery of AAV2 vectors encoding oxidation-resistant apoA1. *Scientific Reports* (2022)
- Choi, YJ et al. Nst1, Densely Associated to P-Body in the Post-Exponential Phases of Saccharomyces cerevisiae, Shows an Intrinsic Potential of Producing Liquid-Like Condensates of P-Body Components in Cells. *International Journal of Molecular Sciences* (2022)
- Császár, E et al. Microglia modulate blood flow, neurovascular coupling, and hypoperfusion via purinergic actions. *The Journal of Experimental Medicine* (2022)
- Tazerart, S et al. Selective activation of BK channels in small-headed dendritic spines suppresses excitatory postsynaptic potentials. *The Journal of Physiology* (2022)
- Weinzierl, A et al. Boosting Tissue Vascularization: Nanofat as a Potential Source of Functional Microvessel Segments. *Frontiers in Bioengineering and Biotechnology* (2022)
- Simon, B et al. Tousled-like kinase 2 targets ASF1 histone chaperones through client mimicry. *Nature Communications* (2022)

- Solovieva, T et al. The embryonic node behaves as an instructive stem cell niche for axial elongation. *Proceedings of the National Academy of Sciences of the United States of America* (2022)
- Zheng S et al. The Cdc42 GTPase activating protein Rga6 promotes the cortical localization of Septin. *J Cell Sci.* (2022)
- Zhang C et al. PKM2 compensates for proteasome dysfunction by mediating the formation of the CHIP-HSP70-BAG3 complex and the aggregation of ubiquitinated proteins. *FASEB J.* (2022)
- Cheng RP et al. Loss of Neuropilin2a/b or Sema3fa alters olfactory sensory axon dynamics and protoglomerular targeting. *Neural Development* (2022)
- Camara A et al. CD169+ macrophages in lymph node and spleen critically depend on dual RANK and LTbetaR signaling. *Proc Natl Acad Sci USA.* (2022)
- Tseng YT et al. The subthalamic corticotropin-releasing hormone neurons mediate adaptive REM-sleep responses to threat. *Neuron.* (2022)
- Dunipace L et al. Brinker levels regulated by a promoter proximal element support germ cell homeostasis. *Development.* (2022)
- Luo YJ et al. Serotonin-1A Receptors Mediate Sex-Dependent Regulation of Neural Stem Cell Expansion and Stress Vulnerability in Adult Hippocampus. *Cell Press Preprint* (2022)
- AlNajjar YT et al. Discovery of novel 6-hydroxybenzothiazole urea derivatives as dual Dyrk1A/α-synuclein aggregation inhibitors with neuroprotective effects. *Eur J Med Chem.* (2022)
- Shankar R et al. The ESCRT machinery directs quality control over inner nuclear membrane architecture. *Cell Rep.* (2022)
- Tung WS et al. PTBP1/HNRNP I controls intestinal epithelial cell regeneration by maintaining stem cell survival and stemness. *bioRxiv Preprint* (2021)
- Lyu P et al. Gene regulatory networks controlling temporal patterning, neurogenesis, and cell-fate specification in mammalian retina. *Cell Rep.* (2021)
- Nagy N et al. Avian ceca are indispensable for hindgut enteric nervous system development. *Development.* (2021)
- Kong JH et al. Gene-teratogen interactions influence the penetrance of birth defects by altering Hedgehog signaling strength. *Development.* (2021)
- Gandhi S et al. A single-plasmid approach for genome editing coupled with long-term lineage analysis in chick embryos. *Development.* (2021)
- Baasch S et al. Cytomegalovirus subverts macrophage identity. *Cell.* (2021)
- Liu H et al. Microglia modulate stable wakefulness via the thalamic reticular nucleus in mice. *Nat Commun.* (2021)
- Denoth-Lippuner A et al. Visualization of individual cell division history in complex tissues using iCOUNT. *Cell Stem Cell.* (2021)
- Akos Z et al. NaNuTrap: a technique for in vivo cell nucleus labelling using nanobodies. *Development.* (2021)
- Li K et al. Patterned endogenous activity controls migration, morphogenesis and survival of adult-born neurons in the mouse olfactory bulb. *bioRxiv Preprint* (2021)
- Estermann MA et al. TGIF1 is required for chicken ovarian cortical development and generation of the juxtacortical medulla. *Development.* (2021)

- Chen Y et al. Wiring logic of the early rodent olfactory system revealed by high-throughput sequencing of single neuron projections. *bioRxiv Preprint* (2021)
- Fabra-Beser J et al. Differential Expression Levels of Sox9 in Early Neocortical Radial Glial Cells Regulate the Decision between Stem Cell Maintenance and Differentiation. *J Neurosci.* (2021)
- Aboushady Y et al. Discovery of Hydroxybenzothiazole Urea Compounds as Multitargeted Agents Suppressing Major Cytotoxic Mechanisms in Neurodegenerative Diseases. *ACS Chem Neurosci.* (2021)
- Omar MH et al. Displacement of PKA catalytic subunit from AKAP signaling islands drives pathology in Cushing's syndrome. *bioRxiv Preprint* (2021)
- Suyama H et al. Top-down acetylcholine signaling via olfactory bulb vasopressin cells contributes to social discrimination in rats. *Commun Biol.* (2021)
- Truong ME et al. Vertebrate cells differentially interpret ciliary and extraciliary cAMP. *Cell.* (2021)
- Ishioka K et al. Upregulation of FGF9 in lung adenocarcinoma transdifferentiation to small cell lung cancer. *Cancer Res.* (2021)
- Ortin-Martinez A et al. Photoreceptor nanotubes mediate the in vivo exchange of intracellular material. *EMBO J.* (2021)
- Kim S et al. Npas4 regulates IQSEC3 expression in hippocampal somatostatin interneurons to mediate anxiety-like behavior. *Cell Rep.* (2021)
- Zhang X et al. Single cell transcriptomic analyses reveal the impact of bHLH factors on human retinal organoid development. *Front Cell Dev Biol.* (2021)
- Abe Y et al. Optical manipulation of local cerebral blood flow in the deep brain of freely moving mice. *Cell Rep.* (2021)
- View More ...

Disclaimer